Int J Adv Manuf Technol (2017) 89:2953–2965
DOI 10.1007/s00170-016-9206-z

ORIGINAL ARTICLE

Development of copper-enriched porous coatings on ternary Ti-Nb-Zr alloy by plasma electrolytic oxidation

Krzysztof Rokosz[1] · **Tadeusz Hryniewicz**[1] · **Steinar Raaen**[2] · **Patrick Chapon**[3] · **Frédéric Prima**[4]

Received: 15 April 2016 / Accepted: 18 July 2016 / Published online: 13 August 2016

Abstract In this paper, a preparation method and characteristics of porous coatings enriched in copper distributed in the whole volume on a ternary Ti-Nb-Zr alloy biomaterial obtained by plasma electrolytic oxidation (PEO) in an electrolyte containing H_3PO_4 within $Cu(NO_3)_2$ at potentials of 180 and 450 V are presented. It has been shown that the PEO potential has impact on the thickness of the coatings, i.e., the higher the potential used, the thicker the coating obtained. Using XPS study, it was shown that copper inside the coating appears as Cu^+ and Cu^{2+} ions, while titanium, niobium, and zirconium appear as Ti^{4+}, Nb^{5+}, and Zr^{x+} ($x \leq 2$), respectively. It was also found that the roughness of PEO coating formed at 450 V is higher than the one obtained at 180 V, and it is well correlated with bigger pores after the PEO treatment. Additionally, in this paper two PEO coating models composed of three sub-layers are presented. The thickness of the outer top porous sub-layer obtained after PEO oxidation at both 180 and 450 V equals to about 2 μm, while the semi-porous as well as transition sub-layers are thicker after PEO processing at 450 V (5 μm) than those obtained at 180 V (4 μm thick). The creation of the top porous and transition compact sub-layer of PEO coating may be explained by switch-on and switch-off of the PEO potential, while the middle and semi-porous sub-layers are most likely formed during the stable voltage conditions of PEO treatment.

Keywords Plasma electrolytic oxidation (PEO) · Micro arc oxidation (MAO) · Titanium ternary Ti-Nb-Zr alloy · SEM · XPS · GDOES · Porous coating

1 Introduction

Among the preparation methods of surface nano-layers with controlled mechanical or electrochemical properties, electropolishing (EP) [1–5], magnetoelectropolishing (MEP) [5–19], and high-current-density electropolishing (HDEP) [20–22] have been previously shown to be highly efficient. The obtained surface nano-layers, which are mostly passive, may be treated as nano-coatings with

✉ Tadeusz Hryniewicz
Tadeusz.Hryniewicz@tu.koszalin.pl

Krzysztof Rokosz
rokosz@tu.koszalin.pl

Steinar Raaen
steinar.raaen@ntnu.no

Patrick Chapon
patrick.chapon@horiba.com

Frédéric Prima
frederic.prima@chimie-paristech.fr

[1] Division of Bioengineering and Surface Electrochemistry, Department of Engineering and Informatics Systems, Koszalin University of Technology, Racławicka 15-17, 75-620 PL Koszalin, Poland

[2] Department of Physics, Norwegian University of Science and Technology (NTNU), Realfagbygget E3-124 Høgskoleringen 5, 7491 NO Trondheim, Norway

[3] HORIBA Jobin Yvon S.A.S, 16-18, rue du Canal, 91165 Longjumeau cedex, France

[4] PSL Research University, ChimieParisTech—CNRS, Institut de Recherche de Chimie Paris, 75005 Paris, France

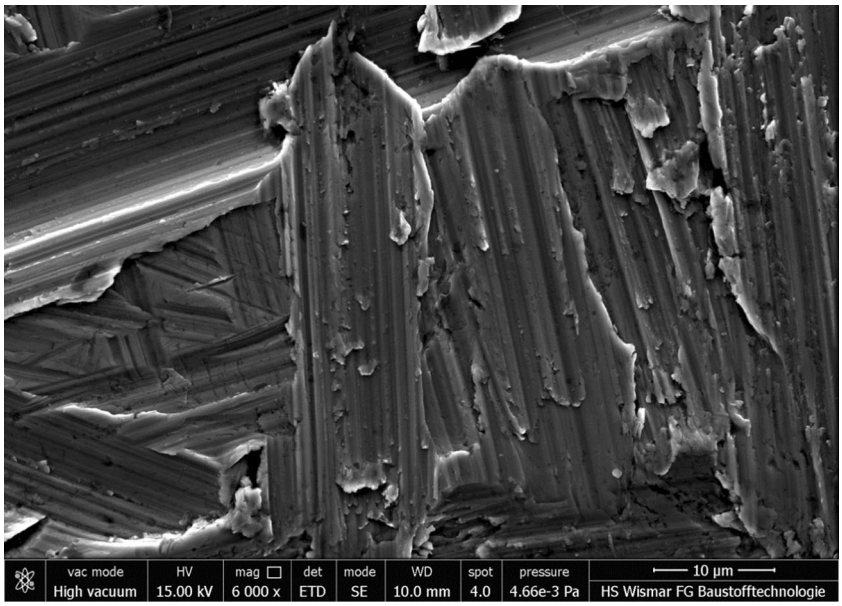

Fig. 1 SEM picture of coating formed on Ti-Nb-Zr after mechanical pretreatment by abrasive paper 120 at ×6000 magnification

determined chemical composition, which is different than that one of matrix. The other method, which can be used to form coatings with micro- and nano-pores, is plasma electrolytic oxidation (PEO). It has been widely used by active companies, such as Keronite (UK), Magoxid-Coat (Germany), and Microplasmic (USA), active in commercial development of PEO technology [23]. Primarily used for pure aluminum or alloyed [23–30] aluminum treatments, PEO was applied recently for the oxidation of magnesium and its alloys [29–33] and titanium and its alloys [34–44] as well as niobium [45–47], zirconium [48–51], and tantalum [52–55]. In recent years, titanium and its alloys used as biomaterials drew the attention of numerous teams of researchers in the world.

A very important point in antibacterial coatings has to be improved for optimized biocompatibility. Some previous papers described the porous and bactericidal coatings on alloys, such as Ti6Al4V [38] and Ti-Nb-Zr-Sn [44] obtained by PEO known also as microarc oxidation (MAO). In those articles, the focal point of analysis was dedicated to the presence of elements displaying a detrimental action in the human body, such as vanadium, aluminum [38, 56, 57], and tin [38, 58].

In the present paper, a "tin-free" Ti-Nb-Zr alloy (TNZ) has been used as a biomaterial substrate for PEO treatments. This ternary titanium alloy was recently extensively studied [38, 43, 44] as a very good candidate for biomedical applications regarding both chemical composition (with fully biocompatible chemical elements) and mechanical properties (with excellent superelastic properties). The main objective of this work is to develop an antibacterial surface layer with porous coating containing mostly phosphates of titanium and/or niobium and/or zirconium within bactericidal copper [59–72] formed on TNZ alloy in an electrolyte consisting of H_3PO_4 within $Cu(NO_3)_2$.

2 Method

2.1 Material

Titanium-niobium-zirconium alloy (Ti-20Nb-6Zr, composition in wt% and at%) samples submitted to PEO (microarc

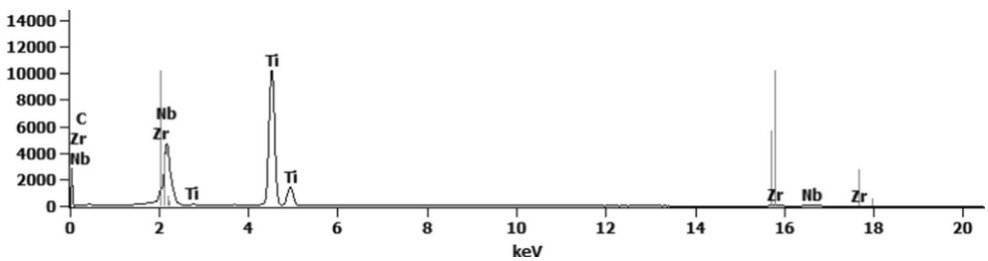

Fig. 2 EDS result of coating formed on Ti-Nb-Zr after mechanical pretreatment by abrasive paper 120 at ×6000 magnification

Table 1 Chemical composition of Ti-Nb-Zr on the basis of EDS measurements

Elements	wt%	wt% ERROR	at%	at% ERROR
Ti K	76.1	± 0.4	85.9	± 0.8
Zr K	7.4	± 1.3	4.4	± 1.6
Nb K	16.5	± 1.8	9.7	± 2.1

oxidation) served for the study. Samples were prepared by mechanical abrasive treatment (Fig. 1) in the form of rectangular specimens of dimensions 35 × 15 mm cut off from a metal sheet 1 mm thick with chemical composition shown in Fig. 2 and Table 1.

2.2 Setup and parameters

The PEO was performed at voltages of 180 ± 10 and 450 ± 10 V, consecutively, during 3 min of processing. A setup used for the studies was presented in our earlier paper [72]. The studies were carried out in the electrolyte of initial temperature of 20 ± 2 °C. For the studies, the electrolyte, i.e., 3.2 mol/L of $Cu(NO_3)_2$ in orthophosphoric acid H_3PO_4, was used. For each run, an electrolytic cell made of glass was used, containing up to 500 mL of the electrolyte.

2.3 SEM and EDS studies

The scanning electron microscope is a Quanta 250 FEI in low vacuum and ESEM mode and a field emission cathode. The

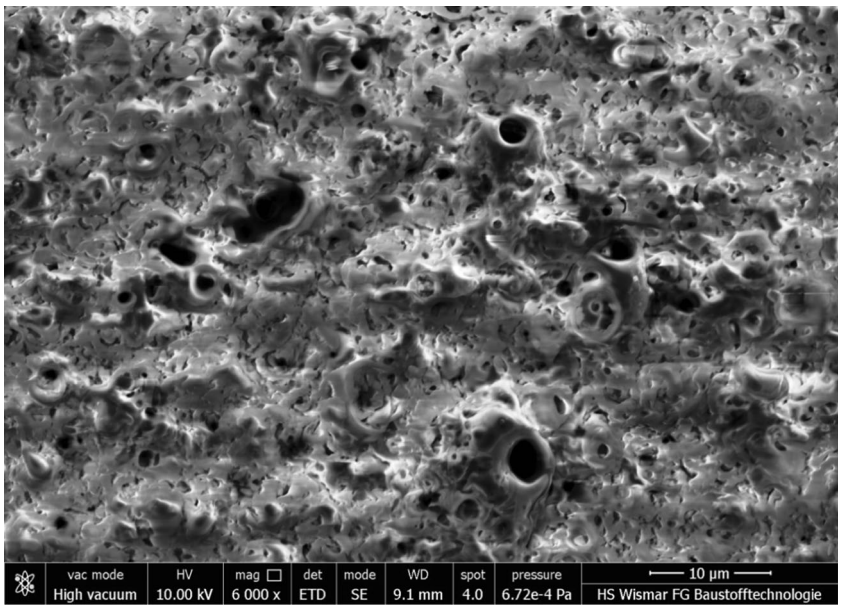

Fig. 3 SEM picture of coating formed on Ti-Nb-Zr after the PEO treatment at voltage of 180 V in 3.2 mol/L of $Cu(NO_3)_2$ in the H_3PO_4 electrolyte. Magnification ×6000

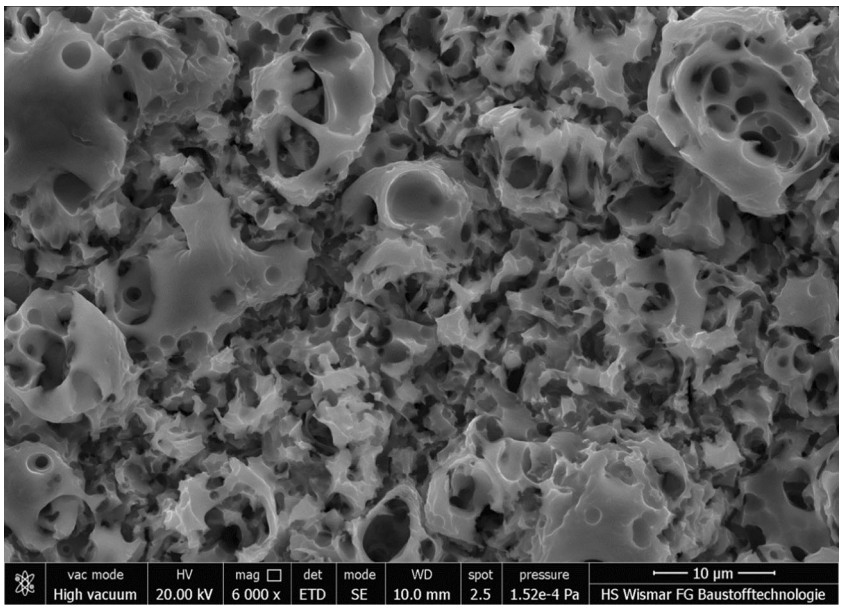

Fig. 4 SEM picture of coating formed on Ti-Nb-Zr after the PEO treatment at voltage of 450 V in 3.2 mol/L of $Cu(NO_3)_2$ in the H_3PO_4 electrolyte. Magnification ×6000

energy-dispersive (EDX) system is a NORAN System SIX with a nitrogen-free silicon drift detector. A ×6000 magnification for SEM images and EDS analyses was used.

2.4 XPS studies

The X-ray photoelectron spectroscopy (XPS) measurements on titanium samples were performed on a SCIENCE SES 2002 instrument using a monochromatic X-ray source Al K(alpha) ($h\nu$ = 1486.6 eV) (18.7 mA, 13.02 kV) (Gammadata Scienta). Scan analyses were carried out with an analysis area of 1 × 3 mm and a pass energy of 500 eV with an energy step 0.2 eV and step time of 200 ms. The binding energy of the spectrometer has been calibrated by the position of the Fermi level on a clean metallic sample. The power supplies were stable and of high accuracy. The experiments were carried out in an ultra-high-vacuum system with a base pressure of about 6×10^{-8} Pa. The XPS spectra were recorded in normal emission. For the XPS analyses, the CasaXPS 2.3.14 software (Shirley background type) [73] with the help of XPS tables [73–79] was used. All the binding energy values presented in this paper were charge-corrected to C 1s at 284.8 eV.

2.5 GDOES studies

The glow discharge optical emission spectroscopy (GDOES) measurements on PEO-oxidized titanium samples were performed by a Horiba Scientific GD-Profiler 2 instrument using an RF asynchronous pulse generator. The operating conditions were as follows: pressure 700 Pa, power 40 W, frequency 3000 Hz, duty cycle 0.25, anode diameter 4 mm. The signals of copper (325 nm), phosphorus (178 nm), oxygen (130 nm), nitrogen (149 nm), hydrogen (122 nm), titanium (365 nm), niobium (316 nm), and zirconium (360 nm) were measured [80].

2.6 2D roughness measurements

A computerized Hommel Tester T800 system of Hommelwerke GmbH was used for measuring the surface roughness, and the GDOES for measuring crater depth. It was equipped with a sliding measuring head Waveline 60 Basic/51808 and a sensor TKL100/17 MO435005. The measuring needle beam was equal to 3.5 μm with an angle of 87°. The tracing, evaluation, and single measuring lengths were equal to 4.8, 4.0, and 0.8 mm, respectively. Due to the porous surface, non-contact methods for surface roughness [81] were not possible to be used, inter alia, because of the uncertainties in measurement results [82]. According to the EN ISO 4287:1999 [83] and DIN 4768 [84] standards, the following roughness parameters have been measured: arithmetic mean of the sum of roughness profile values (Ra), mean peak-to-valley height (Rz^{DIN}), root mean square deviation of the roughness profile (Rq), total height of the roughness profile (Rt), the ratio of the developed profile length to the evaluation length (L_0), and profile peak density (D). All the results were processed by using the software STATISTICA ver. 12 [85].

Table 2 Chemical composition of PEO coating formed on Ti-Nb-Zr treated at two voltages: 180 and 450 V

180 V			450 V		
Elements	wt%	at%	Elements	wt%	at%
P K	34.7	50.8	*P K*	39.8	55.8
Ti K	35.7	33.6	*Ti K*	33.1	30
Nb L	5.3	3.8	*Nb L*	6.7	4.6
Zr L	5.3	2.6	*Zr L*	5.0	2.4
Cu K	19.0	9.2	*Cu K*	15.4	7.2

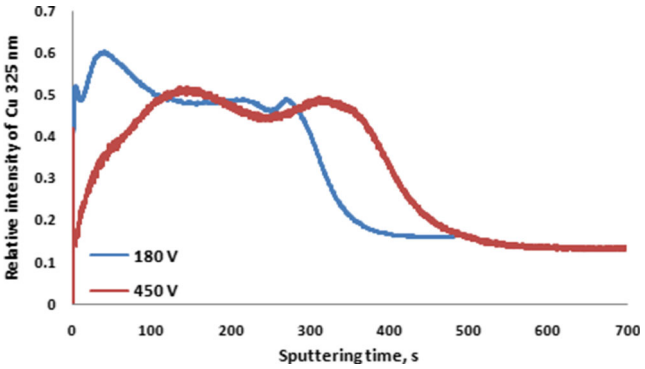

Fig. 5 GDOES results of copper signal (325 nm) of coating formed on Ti-Nb-Zr

3 Results and discussion

In Figs. 3 and 4, the SEM pictures of coating formed on one of the superelastic alloys [86, 87], i.e. the Ti-Nb-Zr alloy surface after PEO treatment at voltages of 180 and 450 V, respectively,

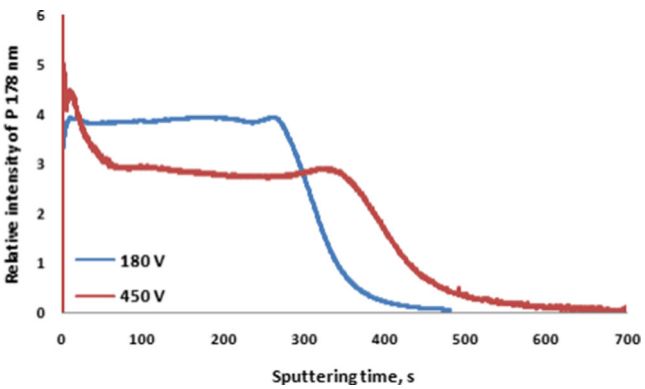

Fig. 6 GDOES results of phosphorus signal (178 nm) of coating formed on Ti-Nb-Zr

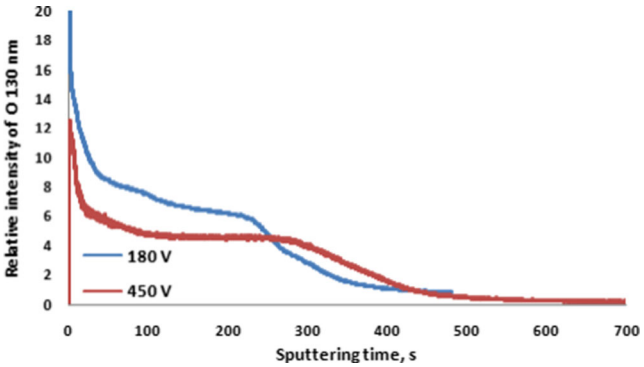

Fig. 7 GDOES results of oxygen signal (130 nm) of coating formed on Ti-Nb-Zr

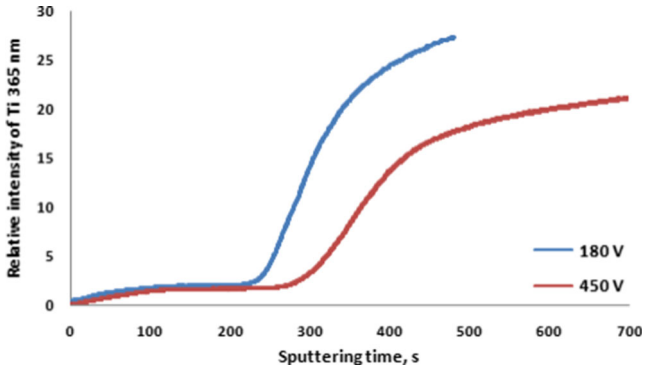

Fig. 10 GDOES results of titanium signal (365 nm) of coating formed on Ti-Nb-Zr

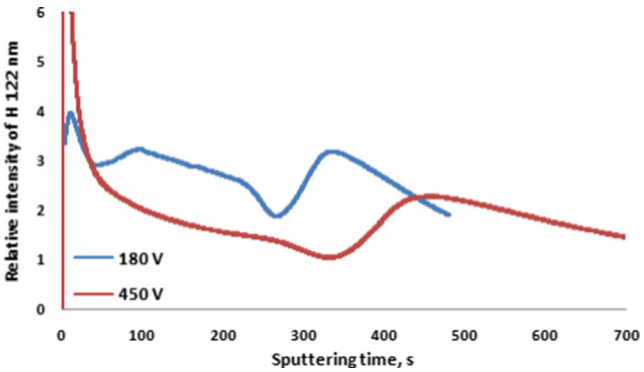

Fig. 8 GDOES results of hydrogen signal (122 nm) of coating formed on Ti-Nb-Zr

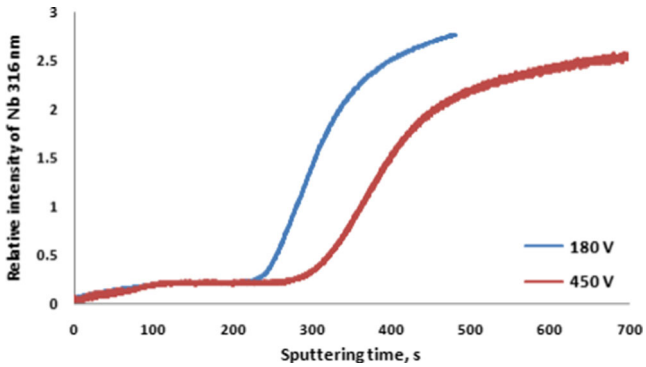

Fig. 11 GDOES results of niobium signal (316 nm) of coating formed on Ti-Nb-Zr

in 3.2 mol/L of $Cu(NO_3)_2$ in H_3PO_4 electrolyte with ×6000 magnifications, are presented. The obtained surface is porous and composed mainly of phosphorus, titanium, and copper within niobium and zirconium. The composition is presented in Table 2. However, the reader must be aware that the EDS signal of phosphorus, niobium, and zirconium are very close to one another. Therefore, the data presented in Table 2 must be treated as orientation ones only. Hence, for comparing the two surfaces, the copper-to-phosphorus (Cu/P) ratio was used. The higher Cu/P ratio was found for oxidation at 180 V, equaling to 0.55. After treatment at 450 V, the ratio was lower (Cu/P = 0.39). The pores are mostly opened in the PEO coating surface after the treatment at 450 V and mostly closed for oxidation at 180 V.

The porous coating obtained after PEO treatment at 450 V has a lot of sharp and open pores (Fig. 4), which are also one within another. The coating grown at 180 V is not so porous as that one formed at 450 V. It is most compact with some craters (Fig. 3). It can suggest that for oxidation at 180 V the pores are mostly closed and developed inside the coating, whereas the PEO treatment at 450 V results in the formation of open pores.

In Figs. 5, 6, 7, 8, 9, 10, 11, and 12, the GDOES depth profiles of copper (325 nm), phosphorus (178 nm), oxygen

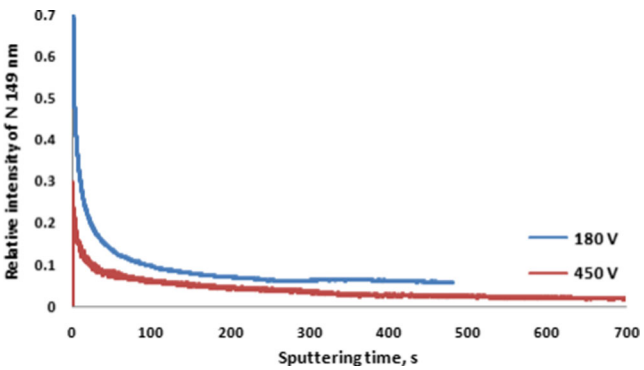

Fig. 9 GDOES results of nitrogen signal (149 nm) of coating formed on Ti-Nb-Zr

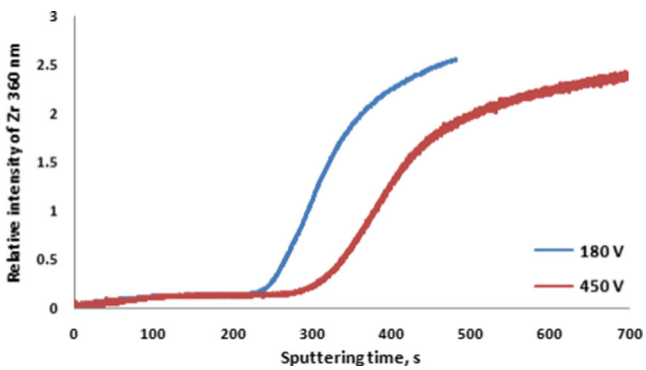

Fig. 12 GDOES results of zirconium signal (360 nm) of coating formed on Ti-Nb-Zr

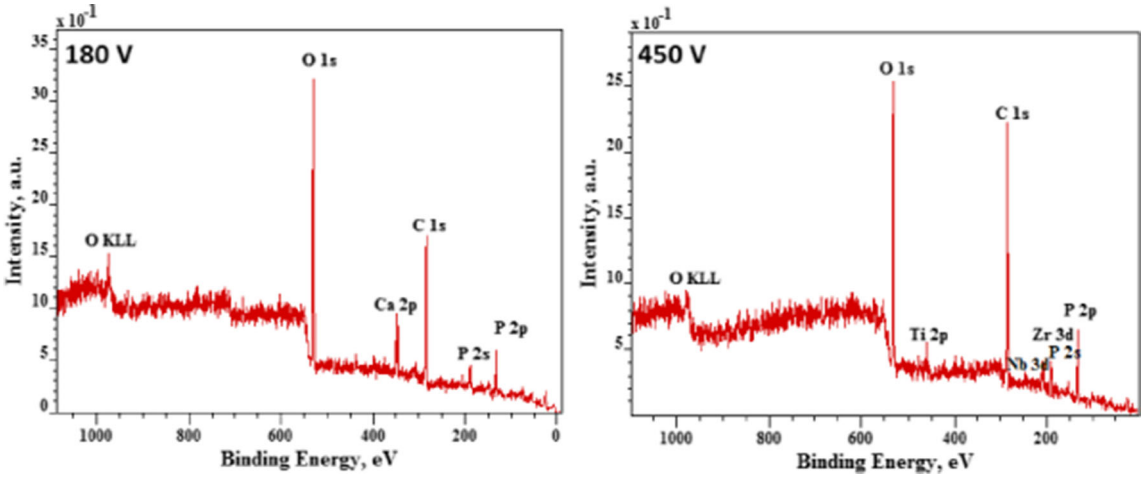

Fig. 13 XPS survey results of coatings formed on Ti-Nb-Zr alloy after 3 min of PEO treatment at voltages 180 and of 450 V in an electrolyte containing H_3PO_4 within $Cu(NO_3)_2$

(130 nm), hydrogen (122 nm), nitrogen (149 nm), titanium (365 nm), niobium (316 nm), zirconium (360 nm), respectively, are presented. The erosion rates slightly evolve with the depth as material changes, but the overall analysis of the GDOES crater indicates that a time of 100 s corresponds to a thickness of about 2 μm.

On the basis of the copper (Fig. 5) and phosphorus (Fig. 6) profiles, it is possible to state that the obtained coatings after PEO consist of three layers. The top one (about 2 μm thick) is enriched in copper for oxidation at 180 V and in phosphorus in case of the treatment at 450 V. The middle layer is thicker after PEO performed at 450 V (about 5 μm) than that after PEO at

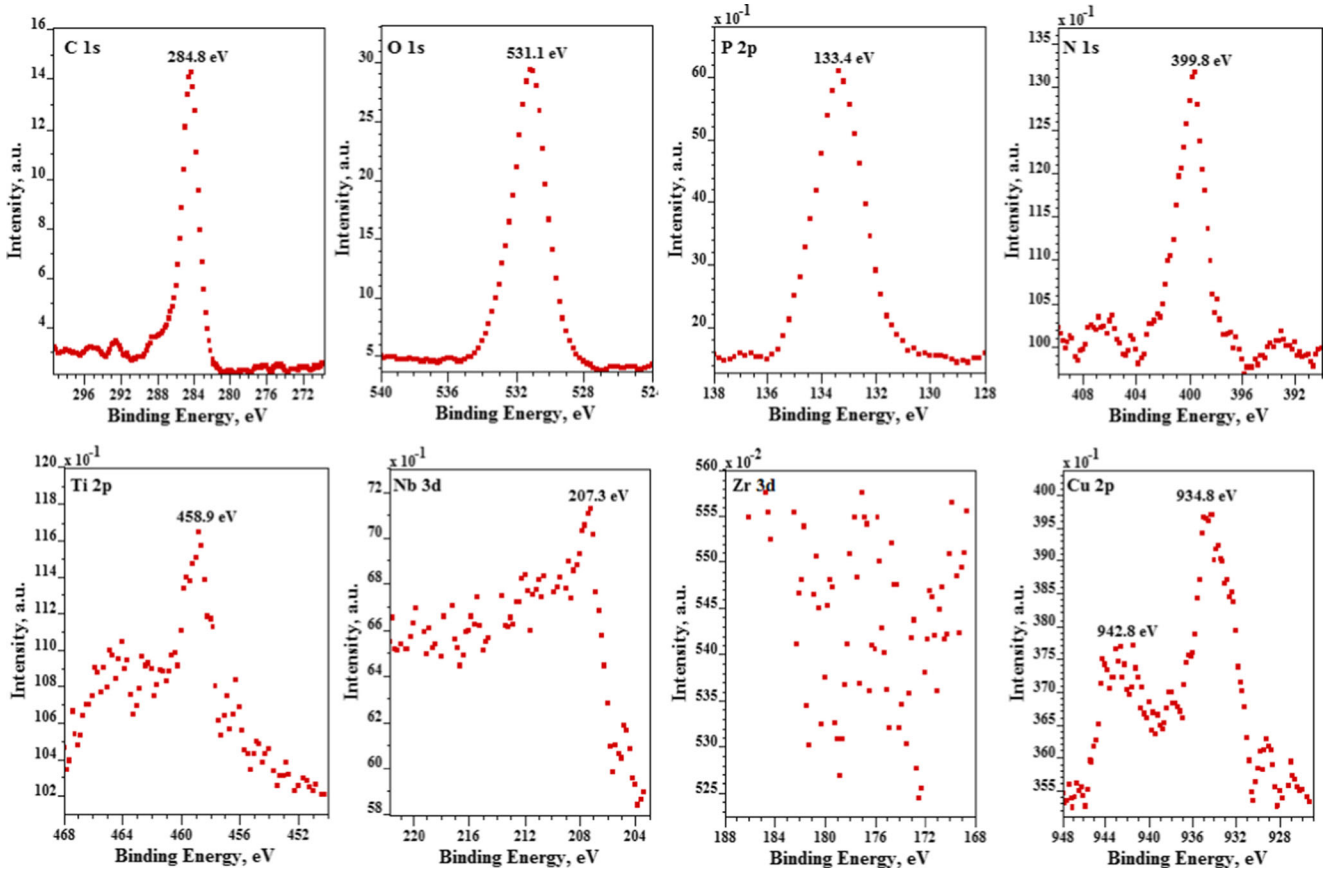

Fig. 14 High-resolution XPS spectra/results of coating formed on Ti-Nb-Zr alloy after 3 min of PEO treatment at voltage of 180 V in the electrolyte containing H_3PO_4 within $Cu(NO_3)_2$

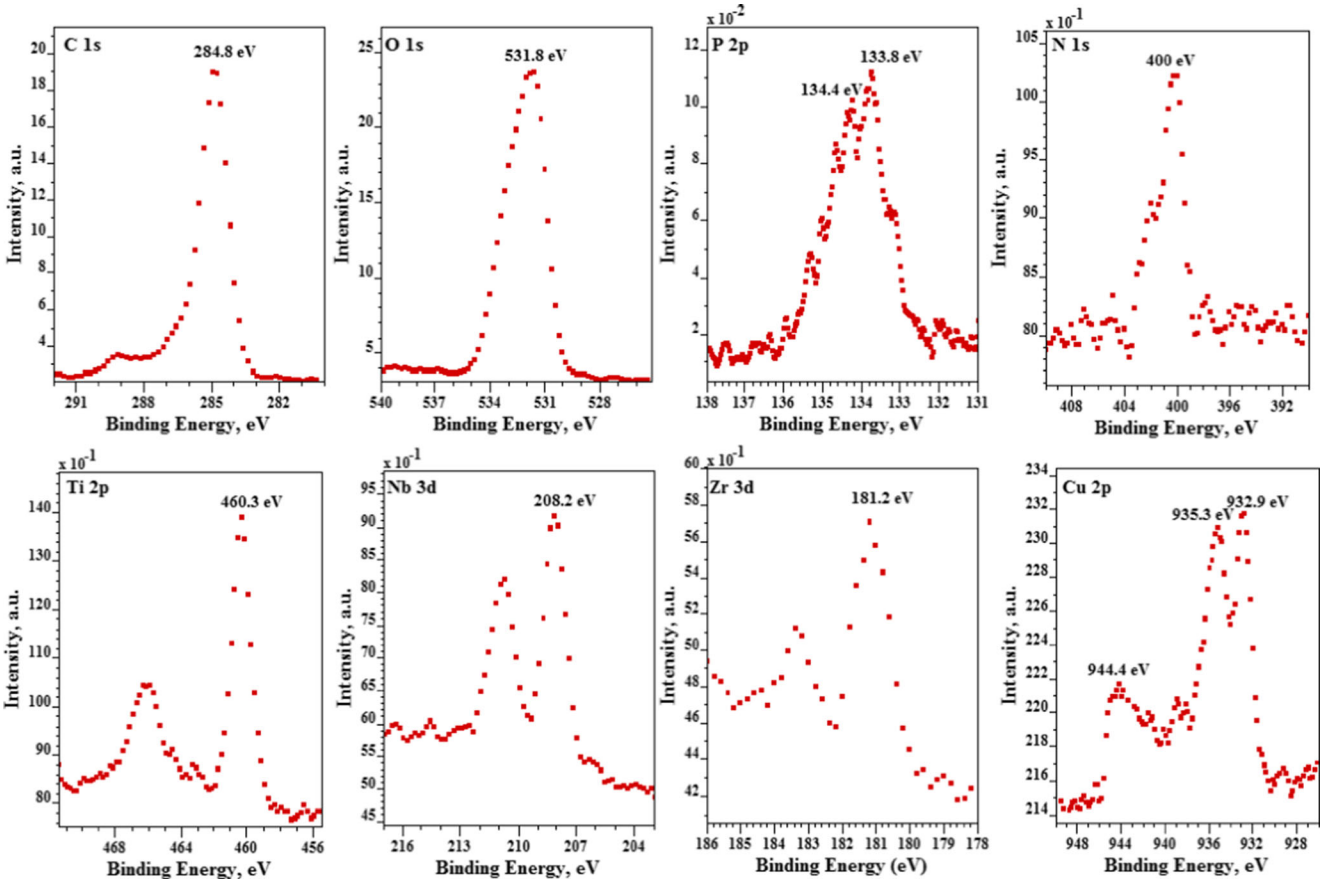

Fig. 15 High-resolution XPS spectra/results of coating formed on Ti-Nb-Zr alloy after 3 min of PEO treatment at voltage of 450 V in the electrolyte containing H_3PO_4 within $Cu(NO_3)_2$

Table 3 Total chemical composition of coating formed after PEO treatment at 180 V on Ti-Nb-Zr alloy with outer carbon contamination and biocontamination sub-layer, at% (based on XPS results)

Titanium	Niobium	Zirconium	Copper	Phosphorus	Oxygen	Nitrogen	Carbon
0.5	0.2	0	0.7	12.2	42.0	2.7	41.7

180 V (about 4 μm thick) with a similar amount of copper inside. The signals of phosphorus (Fig. 6) and oxygen (Fig. 7) are higher after PEO at 180 V than at 450 V, which may be interpreted literally as a higher amount of phosphorus as well as the effect of layer porosity with the depth of analysis. The third inner layer (ca. 4 μm for PEO at 180 V and ca. 5 μm at 450 V) is the interface between the matrix and coating obtained by PEO. The analyses of titanium (Fig. 10), niobium (Fig. 11), and zirconium (Fig. 12) signals confirm the above stated reasoning—thicker coating obtained at a higher voltage (450 V) and existence of the transition layer found in the coating. Additionally, in that layer a peak of hydrogen (Fig. 8) was detected, which may be interpreted as "frozen" in the PEO structure phosphoric acid molecules and/or hydrogen phosphate ions. The spectrum of nitrogen (Fig. 9) is similar after two PEO treatments, and the highest signal was recorded for coating after PEO at 180 V, which

Table 4 Total chemical composition of coating formed after PEO treatment at 450 V on Ti-Nb-Zr alloy with outer carbon contamination and biocontamination sub-layer, at% (based on XPS results)

Titanium	Niobium	Zirconium	Copper	Phosphorus	Oxygen	Nitrogen	Carbon
1.2	0.8	0.2	0.3	0.3	41.4	2.1	54.0

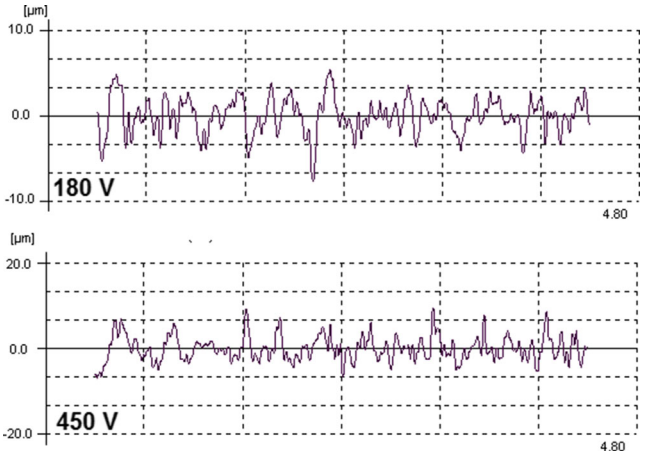

Fig. 16 Two-dimensional profiles of coatings formed on Ti-Nb-Zr alloy after 3 min of PEO treatment at voltages of 180 and 450 V in the electrolyte containing H_3PO_4 within $Cu(NO_3)_2$

confirms the phenomena described in [44]. The detected peaks related to the top surface (top 10 nm) may be explained as surface organic contaminations.

To understand the chemical composition of the top layer (top 10 nm) of PEO coatings, XPS measurements were performed. They are presented in Fig. 13. With XPS, there is no problem separating the phosphorus, niobium, and zirconium signals, as it was the case with EDS. The survey XPS analysis of the PEO coatings obtained at 180 and 450 V indicates that they are composed of phosphorus, titanium, niobium, zirconium, and copper with organic carbon-oxygen contaminations.

To know the oxidation stages of titanium, niobium, zirconium, and copper, high-resolution XPS measurements were performed, and the results are displayed in Figs. 14 and 15. The binding energies of oxygen O 1s (531.1–531.8 eV) and phosphorus P 2p (133.8–134.4 eV) clearly indicate the presence of

Table 5 Roughness parameters of PEO coating formed on Ti-Nb-Zr alloy treated at 180 V for 3 min in 3.2 mol/L of $Cu(NO_3)_2$ in H_3PO_4 electrolytes (the statistics made of five repetitions)

	180 V					
	Ra (µm)	Rz (µm)	Rq (µm)	Rt (µm)	L_o	D
Mean	1.74	10.92	2.27	13.81	1.007	30
Variance	0.04	1.22	0.05	7.91	10^{-7}	29
Standard deviation	0.19	1.10	0.22	2.81	10^{-4}	5
Median	1.62	10.75	2.17	15.16	1.007	31
Maximum	2.01	12.54	2.61	15.88	1.008	35
minimum	1.59	9.49	2.08	9.18	1.006	21
Range	0.43	3.05	0.53	6.7	0.002	14

Ra arithmetic mean of the sum of roughness profile values, Rz^{DIN} mean peak-to-valley height, *Rq* root mean square deviation of the roughness profile, *Rt* total height of the roughness profile, L_0 the ratio of the developed profile length to the evaluation length, *D* profile peak density

Table 6 Roughness parameters of PEO coating formed on Ti-Nb-Zr alloy treated at 450 V for 3 min in 3.2 mol/L of $Cu(NO_3)_2$ in H_3PO_4 electrolytes (the statistics made of five repetitions)

	450 V					
	Ra (µm)	Rz (µm)	Rq (µm)	Rt (µm)	L_o	D
Mean	2.37	15.20	3.10	19.98	1.016	35
Variance	0.02	2.16	0.12	24.27	10^{-6}	14
Standard deviation	0.15	1.47	0.35	4.93	10^{-3}	4
Median	2.32	15.89	2.92	17.62	1.017	35
Maximum	2.56	16.61	3.63	27.31	1.019	39
Minimum	2.20	13.48	2.79	15.83	1.014	31
Range	0.36	3.13	0.84	11.48	0.005	8

Ra arithmetic mean of the sum of roughness profile values, Rz^{DIN} mean peak-to-valley height, *Rq* root mean square deviation of the roughness profile, *Rt* total height of the roughness profile, L_0 the ratio of the developed profile length to the evaluation length, *D* profile peak density

phosphates of titanium and/or niobium and/or zirconium and/or copper in the PEO coatings. The binding energy of carbon (284.8 eV) and nitrogen (399.8–400 eV) can be identified as organic contaminations. The binding energies of the main peaks for titanium Ti $2p_{3/2}$, niobium Nb $3d_{5/2}$, and zirconium Zr $3d_{5/2}$ are equal to 459–460.3, 207.3–208.2, and 181.2 eV*, respectively, which suggests the presence of titanium Ti^{4+}, niobium Nb^{5+}, and zirconium Zr^{x+} ($x \leq 2^*$) [76, 77]. It must be pointed out that the XPS results can be related only to the top 10 nm, therefore they can be treated mainly as a suggestion of oxidation stages, especially in the presence of organic contaminations which provide signals of carbon and nitrogen; they are presented in Tables 3 and 4. The chemical compositions of the studied top nano-layer of the PEO coatings show that for TNZ alloy a higher voltage resulted in formation of a coating containing more oxides than phosphates of titanium and/or niobium and/or copper; it appears that the detected amount of zirconium in this coating is lower than the embedded copper. The amount of copper is higher after the PEO treatment at 180 V; however, because of a high amount of contamination signals (C 1s, N 1s, partly O 1s), it is very hard to state clearly what the chemical composition of this surface layer is, with distinguishing between the contamination layer and the PEO coating.

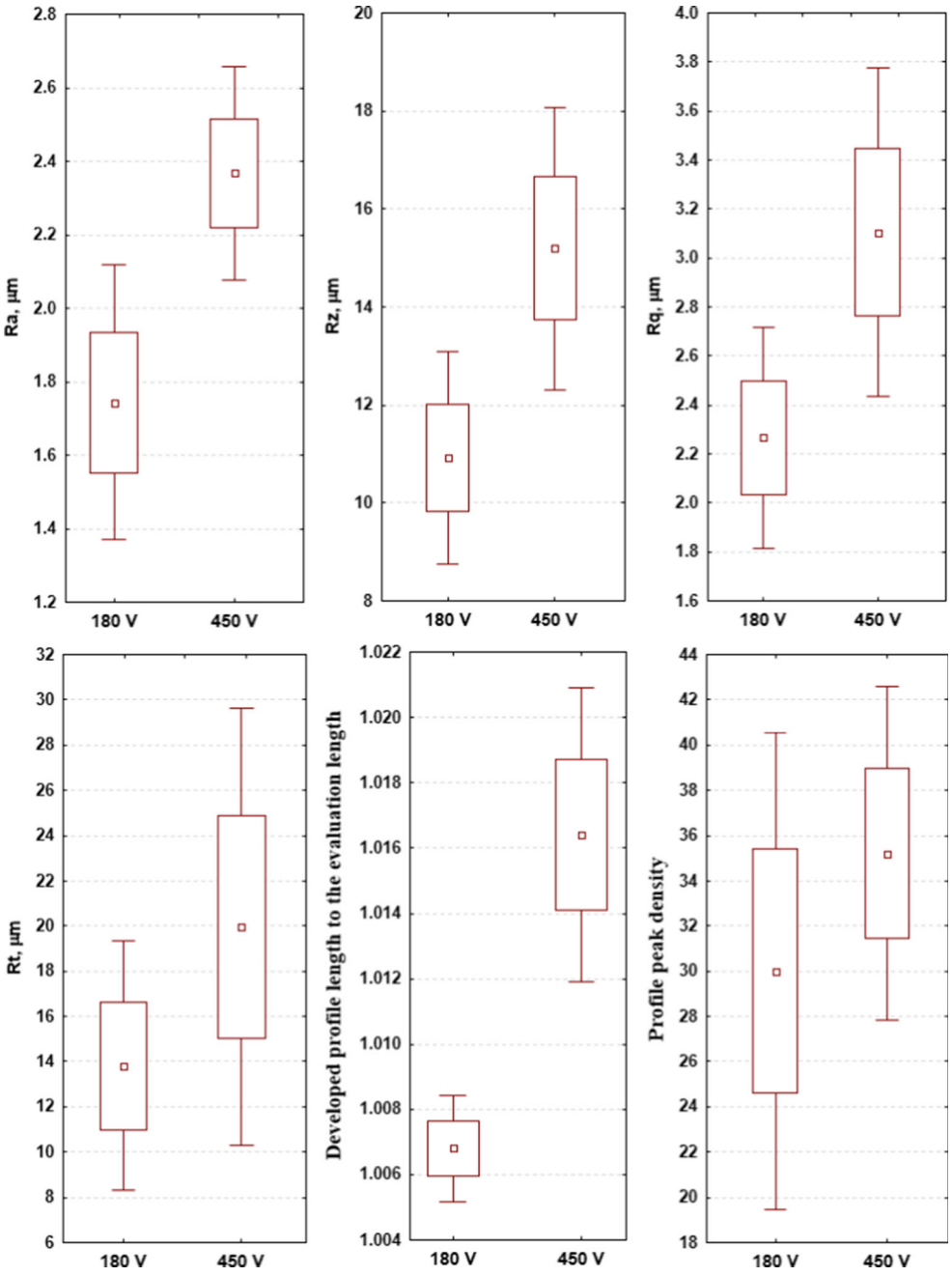

Fig. 17 *Box* and *whisker plots* of the roughness 2D parameters of the surface layer formed on Ti-Nb-Zr alloy after processing at voltages of 180 and 450 V in 3 min of the PEO treatment in the electrolyte containing 3.20 mol/L of $Cu(NO_3)_2$ in H_3PO_4 (the statistics made of three repetitions)

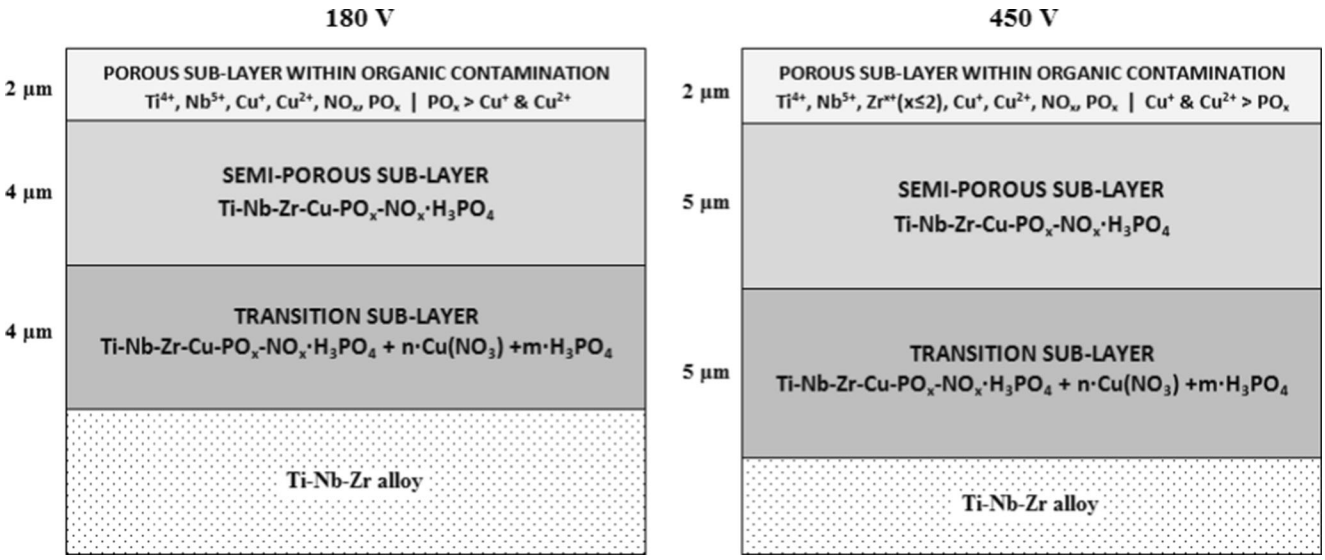

Fig. 18 Models of the coatings formed on Ti-Nb-Zr alloy after 3 min of PEO treatment at voltages of 180 and 450 V, respectively, in the electrolyte containing H_3PO_4 within $Cu(NO_3)_2$

Figure 16 shows the examples of two-dimensional profiles of the coatings formed on TNZ alloy after 3 min of PEO treatment at voltages of 180 and 450 V, consecutively, in the electrolyte composed of H_3PO_4 within $Cu(NO_3)_2$. In Tables 5 and 6 as well as in Fig. 17, the roughness parameters of the PEO coating formed on TNZ alloy at 180 and 450 V, respectively, are presented. Based on these results, it should be concluded that the surface roughness after PEO treatment at 180 V is lower than that after oxidation at 450 V, which was also noted in the case of the PEO of Ti-Nb-Zr-Sn alloy in the same electrolyte [53]. Based on the obtained results, conclusions related to the porosity of the PEO coatings may be drawn, i.e., the higher the roughness parameter, the bigger pores are observed, which was confirmed by SEM and roughness studies (Ra). The significance tests were performed, and that way, the null hypothesis H_0 was formulated. It is assumed that the means of studied populations of roughness parameters are equal for surfaces obtained at two voltages, i.e., 180 and 450 V. Based on the obtained roughness parameters, the probability "p" for all parameters was found. The low probability p from the level of significance (α) indicates that the hypothesis of equality of expected values must be rejected. Proposed 2D roughness parameters such as Ra ($p = 4.21 \times 10^{-4}$), Rz ($p = 8.28 \times 10^{-4}$), Rq ($p = 1.88 \times 10^{-3}$), Rt ($p = 4.1 \times 10^{-2}$), and L ($p = 2.25 \times 10^{-5}$) are significantly different for two surfaces obtained at two voltages (180 and 450 V), and all of them can be used for the evaluation of these surfaces. Only the use of a parameter D ($p = 1.15 \times 10^{-1}$) is not possible in the case of differentiated surfaces after PEO at 180 and 450 V. Roughness parameters such as Ra, Rz, Rq, and L are the best for characterization obtained surfaces, which confirms the probability p and the box and whisker plots in Fig. 17.

Figure 18 shows the models of the coatings formed on Ti-Nb-Zr (TNZ) alloy after 3 min of PEO treatment at voltages of 180 and 450 V in the electrolyte containing H_3PO_4 within $Cu(NO_3)_2$. The two models were created on the basis of GDOES and XPS results presented in this paper. Three sub-layers of PEO coatings are found, i.e., top porous layer with thickness of 2 μm, middle semi-porous layer with thickness of 4–5 μm, and transition compact layer 4–5 μm thick. The model is similar to that one presented in [38]; however, the thicknesses of sub-layers are different. It is also noted that in the transition layer of the present model, one may assume with a high probability that there are molecules of phosphoric acid as the peak of hydrogen in GDOES suggests. Most importantly is the fact that the structure of the obtained models presented in this work is very similar to that given in [38]. This indicates that the obtained results are reproducible and fully reliable.

4 Conclusions

The following conclusions may be formulated after the PEO treatment of tertiary Ti-Nb-Zr alloy studied:

1. Porous coatings on titanium-niobium-zirconium alloy surface, enriched in copper distributed in the whole volume, were obtained.
2. The PEO potential has impact on the thickness of the coatings: the higher the potential used, the thicker coating is obtained.
3. Copper inside the coating appears as Cu^+ and Cu^{2+} ions, while titanium, niobium, and zirconium appear as Ti^{4+}, Nb^{5+}, and Zr^{x+} ($x \leq 2$), respectively.

4. The roughness of PEO coating formed at 450 V is higher than that obtained at 180 V, and it is well correlated with bigger pores obtained after the PEO treatment.
5. Three sub-layers, i.e., outer (porous), inner (semi-porous), and transition (adjacent to the matrix), may be separated in the PEO coating formed on Ti-Nb-Zr alloy.
6. The thickness of the outer top porous sub-layer obtained after PEO oxidation at both 180 and 450 V equals to about 2 μm, while the semi-porous as well as transition sub-layers are thicker after PEO processing at 450 V (5 μm) than those obtained at 180 V (4 μm).
7. It is most likely that the transition sub-layer, adjacent to the matrix, is formed at the very beginning of PEO treatment (switch-on of the PEO potential) and the outer, porous sub-layer, is formed at the end of PEO treatment (switch-off of the PEO potential), while the second, semi-porous sub-layer, is formed during the stable voltage conditions of PEO treatment.

Acknowledgments Prof. Dr. Ing. Wienfried Malorny of Hochschule Wismar, Germany, is greatly acknowledged for making his labs accessible and for valuable advices for SEM and EDS studies. Many thanks are directed to Professor Czesław Łukianowicz, DSc PhD, the Dean at the Faculty of Mechanical Engineering of KUT, for making available a computerized Hommel Tester T800 system of Hommelwerke GmbH.

References

1. Hryniewicz T (1994) Concept of microsmoothing in the electropolishing process. Surf Coat Technol 64:75–80
2. Rokicki R, Hryniewicz T (2012) Enhanced oxidation-dissolution theory of electropolishing. Trans Inst Met Finish 90(4):188–196
3. Hryniewicz T (2007) On the surface treatment of metallic biomaterials. Koszalin University of Technology Publishing(in Polish), (155 pages)
4. Hryniewicz T, Rokosz K, Zschommler Sandim HR (2012) SEM/EDX and XPS studies of niobium after electropolishing. Appl Surf Sci 263:357–361
5. Rokosz K (2012) Electrochemical polishing in magnetic field (Polerowanie elektrochemiczne w polu magnetycznym). Koszalin University of Technology Publishing in Polish
6. Hryniewicz T, Rokicki R, Rokosz K (2008) Co-Cr alloy corrosion behaviour after electropolishing and "magnetoelectropolishing" treatments. Surf Coat Technol 62(17–18):3073–3076
7. Hryniewicz T, Rokosz K (2010) Analysis of XPS results of AISI 316L SS electropolished and magnetoelectropolished at varying conditions. Surf Coat Technol 204(16–17):2583–2592
8. Hryniewicz T, Rokicki R, Rokosz K (2007) Magnetoelectropolishing for metal surface modification. Trans Inst Met Finish 85(6):325–332
9. Rokicki R, Hryniewicz T (2008) Nitinol surface finishing by magnetoelectropolishing. Trans Inst Met Finish 86:280–285
10. Hryniewicz T, Rokicki R, Rokosz K (2008) Corrosion and surface characterization of titanium biomaterial after magnetoelectropolishing. Surf Coat Technol 203(9):1508–1515
11. Hryniewicz T, Rokosz K (2010) Polarization characteristics of magnetoelectropolishing stainless steels. Mater Chem Phys 122(1):169–174
12. Rokosz K, Hryniewicz T, Raaen S (2012) Characterization of passive film formed on AISI 316L stainless steel after magnetoelectropolishing in a broad range of polarization parameters. J Iron Steel Res 83(9):910–918
13. Hryniewicz T, Rokosz K, Rokicki R (2013) Magnetic fields for electropolishing improvement: materials and systems. Int Lett Chem Phys Astron 23(11):98–108. doi:10.18052/www.scipress.com/ILCPA.23.98
14. Hryniewicz T, Rokosz K (2010) Investigation of selected surface properties of AISI 316L SS after magnetoelectropolishing. Mater Chem Phys 123(1):47–55. doi:10.1016/j.matchemphys.2010.03.060
15. Hryniewicz T, Rokosz K (2014) Corrosion resistance of magnetoelectropolished AISI 316L SS biomaterial. Anti-Corros Methods Mater 61(2):57–64
16. Hryniewicz T, Rokosz K, Valiček J, Rokicki R (2012) Effect of magnetoelectropolishing on nanohardness and Young's modulus of titanium biomaterial. Mater Lett 83:69–72
17. Hryniewicz T, Rokosz K, Rokicki R, Prima F (2015) Nanoindentation and XPS studies of titanium TNZ alloy after electrochemical polishing in a magnetic field. Materials 8:205–215
18. Rokosz R, Hryniewicz T, Simon F, Rzadkiewicz S (2015) XPS analysis of AISI 304L stainless steel surface after electropolishing. Adv Mater Sci 15(1):21–29. doi:10.1515/adms-2015-0004
19. Rokicki R, Haider W, Hryniewicz T (2012) Influence of sodium hypochlorite treatment of electropolished and magnetoelectropolished nitinol surfaces on adhesion and proliferation of MC3T3 pre-osteoblast cells. J Mater Sci Mater Med 23:2127–2139. doi:10.1007/s10856-012-4696-1
20. Rokosz K, Hryniewicz T, Simon F, Rzadkiewicz S (2015) Comparative XPS analysis of passive layers composition formed on AISI 304L SS after standard and high-current density electropolishing. Surf Interface Anal 47(1):87–92
21. Rokosz R, Hryniewicz T, Rzadkiewicz S, Raaen S (2015) High-current-density electropolishing (HDEP) of AISI 316L SS (EN 1.4404) stainless steel. Tehnicki vjesnik-Technical Gazette 22(2):415–424. doi:10.17559/TV-20140722110711
22. Rokosz K, Lahtinen J, Hryniewicz T, Rzadkiewicz S (2015) XPS depth profiling analysis of passive surface layers formed on austenitic AISI 304L and AISI 316L SS after high-current-density electropolishing. Surf Coat Technol 276:516–520
23. Dehnavi V (2014) Surface modification of aluminum alloys by plasma electrolytic oxidation. University of Western Ontario-Electronic Thesis and Dissertation Repository, paper 2311. 216 pages
24. Klapkiv MD, Nykyforchyn HM, Posuvailo VM (1994) Spectral analysis of an electrolytic plasma in the process of synthesis of aluminium oxide. Mater Sci 30:333–343
25. Yerokhin AL, Nie X, Leyland A, Matthews A, Dowey SJ (1999) Plasma electrolysis for surface engineering. Surf Coat Technol 122(2–3):73–93
26. Dehnavi V, Liub XY, Luan BL, Shoesmith DW, Rohani S (2014) Phase transformation in plasma electrolytic oxidation coatings on 6061 aluminum alloy. Surf Coat Technol 251:106–114
27. Dehnavi V, Luan BL, Shoesmith DW, Liu XY, Rohani S (2013) Effect of duty cycle and applied current frequency on plasma electrolytic oxidation (PEO) coating growth behavior. Surf Coat Technol 226:100–107
28. Cheng Y-l, Xue Z-G, Wang Q, Wua X-Q, Matykina E, Skeldon P, Thompson GE New findings on properties of plasma electrolytic

oxidation coatings from study of an Al–Cu–Li alloy. Electrochim Acta 107:358–378
29. Walsh FC, Low CTJ, Wood RJK, Stevens KT, Archer J, Poeton AR, Ryder A (2009) Review. Plasma electrolytic oxidation (PEO) for production of anodised coatings on lightweight metal (Al, Mg, Ti) alloys. Trans Inst Met Finish 87:122–135
30. Curran J (2011) Plasma electrolytic oxidation for surface protection of aluminium, magnesium and titanium alloys. Trans Inst Met Finish 89:295–297
31. Hussein RO, Northwood DO, Nie X (2014) Processing-microstructure relationships in the plasma electrolytic oxidation (PEO) coating of a magnesium alloy. Mater Sci Appl 5:124–139
32. Hussein RO, Nie X, Northwood DO (2013) The application of plasma electrolytic oxidation (PEO) to the production of corrosion resistant coatings on magnesium alloys: a review. Corros Mater 38: 55–65
33. Liang J, Srinivasan PB, Blawert C, Stormer M, Dietzel W (2009) Electrochemical corrosion behaviour of plasma electrolytic oxidation coatings on AM50 magnesium alloy formed in silicate and phosphate based electrolytes. Electrochim Acta 54:3842–3850
34. Han Y, Hong SH, Xu KW (2002) Synthesis of nanocrystalline titania films by micro-arc oxidation. Mater Lett 56:744–747
35. Han Y, Hong SH, Xu KW (2002) Porous nanocrystalline titania films by plasma electrolytic oxidation. Surf Coat Technol 154: 314–318
36. Simka W, Sadowski A, Warczak M, Iwaniak A, Dercz G, Michalska J, Maciej A Modification of titanium oxide layer by calcium and phosphorus. Electrochim Acta 56(24):8962–8968
37. Rokosz K, Hryniewicz T, Dudek Ł, Matysek D, Valiček J, Harničarova M (2016) SEM and EDS analysis of surface layer formed on titanium after plasma electrolytic oxidation in H_3PO_4 with the addition of $Cu(NO_3)_2$. J Nanosci Nanotechnol 16(8): 7814–7817
38. Rokosz K, Hryniewicz T, Raaen S (2016) Development of plasma electrolytic oxidation for improved Ti6Al4V biomaterial surface properties. Int J Adv Manuf Technol. doi:10.1007/s00170-015-8086-y
39. Wang Y, Jia D, Guo L, Lei T, Jiang B (2005) Effect of discharge pulsating on microarc oxidation coatings formed on Ti-6Al-4V alloy. Mater Chem Phys 90:128–133
40. Hussein RO, Nie X, Northwood DO (2012) A spectroscopic and microstructural study of oxide coatings produced on a Ti-6Al-4V alloy by plasma electrolytic oxidation. Mater Chem Phys 134:484–492
41. Krząkała A, Młyński J, Dercz G, Michalska J, Maciej A, Nieużyla L, Simka W (2014) Modification of Ti-6Al-4V alloy surface by EPD-PEO process in $ZrSiO_4$ suspension. Arch Metall Mater 59(1):199–204
42. Simka W, Nawrat G, Chlode J, Maciej A, Winiarski A, Szade J, Radwanski K, Gazdowicz J (2011) Electropolishing and anodic passivation of Ti6Al7Nb alloy. Przem Chem 90(1):84–90
43. Rokosz K, Hryniewicz T (2015) Characteristics of porous biocompatible coatings obtained on niobium and titanium-niobium-zirconium (TNZ) alloy by plasma electrolytic oxidation. Mechanik 12:15–18
44. Rokosz K, Hryniewicz T, Raaen S, Chapon P (2016) Investigation of porous coatings obtained on Ti-Nb-Zr-Sn alloy biomaterial by plasma electrolytic oxidation: characterisation and modelling. Int J Adv Manuf Technol. doi:10.1007/s00170-016-8692-3
45. Norlin A (2005) Porous niobium oxide as electrode material and manufacturing process US 20090292346:A1
46. Sowa M, Kazek-Kęsik A, Krząkała A, Socha RP, Dercz G, Michalska J, Simka W (2014) Modification of niobium surfaces using plasma electrolytic oxidation in silicate solutions. J Solid State Electrochem 18(11):3129–3142
47. Simka W (2013) Habilitation summary of professional accomplishments (in Polish). Chemical Engineering Department, Silesian University of Technology (Wydział Chemiczny Politechniki Śląskiej), Gliwice, pp. 1–18
48. Bajat J, Mišković-Stanković V, Vasilić R, Stojadinović S (2014) Corrosion evaluation of zirconium doped oxide coatings on aluminum formed by plasma electrolytic oxidation. Acta Chim Slov 61(2):308–315
49. Chen Y, Nie X, Northwood DO (2009) Plasma electrolytic oxidation (PEO) coatings on a zirconium alloy for improved wear and corrosion resistance. New nuclear frontiers 30th Annual Canadian Nuclear Society Conference and 33rd CNS/CNA Student Conference, (p. 275Megabytes). Canada: Canadian Nuclear Society. ISBN 0-919784-95-X
50. Xue W, Zhu Q, Jin Q, Hua M (2010) Characterization of ceramic coatings fabricated on zirconium alloy by plasma electrolytic oxidation in silicate electrolyte. Mater Chem Phys 120:656–660
51. Matykina E, Arrabal R, Skeldon P, Thompson GE, Wang P, Wood P (2010) Plasma electrolytic oxidation of a zirconium alloy under AC conditions. Surf Coat Technol 204:2142–2151
52. Sowa M, Kazek-Kęsik A, Socha RP, Dercz G, Michalska J, Simka W (2013) Modification of tantalum surface via plasma electrolytic oxidation in silicate solutions. Electrochim Acta 114:627–636
53. Wang CC, Wang F, Han Y (2015) The structure, bond strength and apatite-inducing ability of micro-arc oxidized tantalum and their response to annealing. Appl Surf Sci 361:190–198
54. Petković M, Stojadinović S, Vasilić R, Belča I, Kasalica B, Zeković L (2012) Plasma electrolytic oxidation of tantalum. Serbian J Electr Eng 9(1):81–94
55. Petković M, Stojadinović S, Vasilić R, Zeković L (2011) Characterization of oxide coatings formed on tantalum by plasma electrolytic oxidation in 12-tungstosilicic acid. Appl Surf Sci 257: 10590–10594
56. Ku CH, Pioletti DP, Browne M, Gregson PJ (2002) Effect of different Ti–6Al–4V surface treatments on osteoblasts behaviour. Biomaterials 23:1447–1454
57. Bellows CG, Heersche JN, Aubin JE (1999) Aluminium accelerates osteoblastic differentiation but is cytotoxic in long-term rat calvaria cell cultures. Calcif Tissue Int 65:59–65
58. Winship KA (1988) Toxicity of tin and its compounds. Adverse Drug React Acute Poisoning Rev 7(1):19–38
59. Dollwet H, Sorenson J (2012) Historic uses of copper compounds in medicine. Trace Elem Med 2(2):80–87
60. Stanića V, Dimitrijević S, Antić-Stanković J, Mitrića M, Jokić B, Plećaš IB, Raičević S (2010) Synthesis, characterization and antimicrobial activity of copper and zinc doped hydroxyapatite nanopowder. Appl Surf Sci 256(20):6083–6089
61. Yang H, Zhang L, Xu K-W (2009) Effect of storing on the microstructure of Ag/Cu/HA powder. Ceram Int 35(4):1595–1601
62. White C, Lee J, Kambe T, Fritsche K, Petris MJ (2009) A role for the ATP7A copper-transporting ATPase in macrophage bactericidal activity. J Biol Chem 284(49):33949–33956
63. Xiangyu Z, Xiaobo H, Ma Y, Lin N, Ailan F, Bin T (2012) Bactericidal behavior of Cu-containing stainless steel surfaces. Appl Surf Sci 258:10058–10063
64. Xiaohong Y, Xiangyug Z, Haibo W, Linhai T, Yong M, Bin T (2014) Microstructure and antibacterial properties of Cu-doped TiO_2 coating on titanium by micro-arc oxidation. Appl Surf Sci 292:944–947. doi:10.1016/j.apsusc.2013.12.083
65. Hempel F, Finke B, Zietz C, Bader R, Weltmann KD, Polak M (2014) Antimicrobial surface modification of titanium substrates by means of plasma immersion ion implantation and deposition of copper. Surf Coat Technol 256:52–58. doi:10.1016/j.surfcoat.2014.01.027
66. Zhua W, Zhang Z, Gu B, Sun J, Zhu L (2013) Biological activity and antibacterial property of nano-structured TiO_2 coating

incorporated with Cu prepared by micro-arc oxidation. J Mater Sci Technol 29(3):237–244. doi:10.1016/j.jmst.2012.12
67. Osman D, Waldron KJ, Denton H, Taylor CM, Grant AJ, Mastroeni P, Robinson NJ, Cavet JS (2010) Copper homeostasis in Salmonella is atypical and copper-cups is a major periplasmic metal complex. J Biol Chem 285(33):25259–25268
68. Soutourina O, Dubrac S, Poupel O, Msadek T, Martin-Verstraete I (2010) The pleiotropic CymR regulator of *Staphylococcus aureus* plays an important role in virulence and stress response. PLoS Pathog 6(5):e1000894. doi:10.1371/journal.ppat.1000894
69. Wolschendorf F, Ackart D, Shrestha TB, Hascall-Dove L, Nolan S, Lamichhane G, Wang Y, Bossmann SH, Basaraba RJ, Niederweis M (2011) Copper resistance is essential for virulence of Mycobacterium tuberculosis. Proc Natl Acad Sci U S A 108(4): 1621–1626
70. Babu U, Failla ML (1990) Respiratory burst and candidacidal activity of peritoneal macrophages are impaired in copper deficient rats. J Nutr 120(12):1692–1699
71. Li Y, Ho J, Ooi CP (2010) Antibacterial efficacy andcytotoxicity studies of copper (II) and titanium (IV) substituted hydroxyapatite nanoparticles. Mater Sci Eng C 30(8):1137–1144
72. Rokosz K, Hryniewicz T (2016) Plasma electrolytic oxidation as a modern method to form porous coatings enriched in phosphorus and copper on biomaterials. World Sci News 35:44–61
73. Casa Software Ltd (2009) CasaXPS: processing software for XPS. AES, SIMS and More http://www.casaxps.com. Accessed 29 Mar 2016
74. Biesinger MC, Lau LWM, Gerson AR, Smart RSC (2010) Resolving surface chemical states in XPS analysis of first row transition metals, oxides and hydroxides: Sc, Ti, V, Cu and Zn. Appl Surf Sci 257:887–898. doi:10.1016/j.apsusc.2010.07.086
75. Rodenbücher CH (2014) Resistive switching phenomena of extended defects in Nb-doped $SrTiO_3$ under influence of external gradients. Forschungszentrum Julich, Dissertation 38 RWTH Aachen University, ISSN 1866-1777, ISBN 978-3-89336-980-5, 79–80
76. Wagner CD, Naumkin AV, Kraut-Vass A, Allison JW, Powell CJ, Rumble JR Jr (2003) NIST standard reference database 20, version 3.4
77. (2003) http://srdata.nist.gov/xps. Accessed 29 Mar 2016
78. Boffa AB (1994) Transition metal oxides deposited on rhodium and platinum: surface chemistry and catalysis, center for advanced materials, Lawrence Berkeley Laboratory, University of California, PhD Thesis, LBL-35954, UC-401
79. Ismail M, Huang C-Y, Panda D, Hung C-J, Tsai T-L, Jieng J-H, Lin C-A, Chand U, Rana AM, Ahmed E, Talib I, Nadeem MY, Tseng T-Y (2014) Forming-free bipolar resistive switching in nonstoichiometric ceria films. Nanoscale Res Lett 9(45):1–8
80. Pulsed RF Glow Discharge Optical Emission Spectrometry—Ultra Fast Elemental Depth Profiling (2014) HORIBA Scientific, Printed in France—©HORIBA Jobin Yvon: 7 pages. http://www.horiba.com/scientific/products/atomic-emission-spectroscopy/glow-discharge/. Accessed 29 Mar 2016
81. Valiček J, Drzik M, Hryniewicz T, Harničarova M, Rokosz K, Kušnerova M, Barcova K, Brazina D (2012) Non-contact method for surface roughness measurement after machining. Meas Sci Rev 12(5):184–188. doi:10.2478/v10048-012-0028-3
82. Kušnerova M, Valiček J, Harničarova M, Hryniewicz T, Rokosz K, Palkova Z, Vaclavik V, Repka M, Bendova M (2013) A proposal for simplifying the method of evaluation of uncertainties in measurement results. Meas Sci Rev 13(1):1–6. doi:10.2478/msr-2013-0007
83. EN ISO 4287:1999 Geometrical product specifications (GPS)—surface texture: profile method—terms, definitions and surface texture parameters
84. DIN 4768 comparison of surface roughness values
85. StatSoft, Inc. STATISTICA (data analysis software system), version 12. www.statsoft.com
86. Zhang JY, Sun F, Hao YL, Gozdecki N, Lebrun E, Vermaut P, Portier R, Gloriant T, Laheurte P, Prima F (2013) Influence of equiatomic Zr/Nb substitution on superelastic behavior of Ti-Nb-Zr alloy. Mater Sci Eng A 563:78–85
87. Sun F, Hao YL, Nowak S, Gloriant T, Laheurte P, Prima F (2011) A thermo-mechanical treatment to improve the superelastic performances of biomedical Ti-26Nb and Ti-20Nb-6Zr (at.%) alloys. J Mech Behav Biomed Mater 4(8): 1864–1872